Journal of Hydrology 496 (2013) 178–186

Contents lists available at SciVerse ScienceDirect

Journal of Hydrology

journal homepage: www.elsevier.com/locate/jhydrol

Source and magnitude of error in an inexpensive image-based water level measurement system

Troy E. Gilmore [a,*], François Birgand [a], Kenneth W. Chapman [b]

[a] Biological and Agricultural Engineering Dept., North Carolina State University, Raleigh, NC 27695, USA
[b] GaugeCam, 1205 Verde Farm Rd., Raleigh, NC 27603, USA

ARTICLE INFO

Article history:
Received 15 November 2011
Received in revised form 21 January 2013
Accepted 5 May 2013
Available online 16 May 2013
This manuscript was handled by Konstantine P. Georgakakos, Editor-in-Chief, with the assistance of Emmanouil N. Anagnostou, Associate Editor

Keywords:
Water level
Water stage
Machine vision
Edge detection
Instrument comparison
Uncertainty

SUMMARY

Recent technological advances have opened the possibility to use webcams and images as part of the environmental monitoring arsenal. The potential sources and magnitude of uncertainties inherent to an image-based water level measurement system are evaluated in an experimental design in the laboratory. Sources of error investigated include image resolution, lighting effects, perspective, lens distortion and water meniscus. Image resolution and meniscus were found to weigh the most in the overall uncertainty of this system. Image distortion, although largely taken into account by the software developed, may also significantly add to uncertainty. Results suggest that "flat" images with little distortion are preferable. After correction for the water meniscus, images captured with a camera (12 mm or 16 mm focal lengths) positioned 4–7 m from the water level edge have the potential to yield water level measurements within ±3 mm when using this technique.

1. Introduction

Water level measurement is a critical component for observation and management of water resources. Water supply volumes, storm water discharge, and nutrient transport rates are all commonly calculated based on water level measurements. Heiner et al. (2011) investigated seventy installed flow measurement devices, the vast majority of which depended on water height to calculate discharge, and found that 67% of produced measurements were outside of the design error. In many cases, this was due to improper installation or maintenance of the control structures onsite. In addition to installation and maintenance, the impact of changing hydrologic conditions such as weir submergence or backwater conditions (Rantz et al., 1983) are often unknown unless maintenance or research personnel are onsite. An image-based water level measurement instrument will not correct improper installation or maintenance of control structures. However, the user of an image-based water level measurement system has access to additional information, which can be 'visually' verified and interpreted with the human eye, providing tremendous additional value to the current techniques. Hauet et al. (2008b) added that an image-based water level measurement system would be ideal for measuring river stage as part of a field-based particle image velocimetry (PIV) system.

Because the interpretation of the raw data is performed away from the field (real time or after collection on an SD card), the proposed image-based system does not require on-site calibration and for that reason involves only low skill maintenance such as cleaning the camera lens, and ensuring a clean and plumb target background. This opens the possibility for communities (e.g. flood prone areas) where no hydrological expertise is available to obtain their own verifiable and easily understandable hydrological data. The image-based water level measurement system presented here is to be used in the field and the uncertainties for these conditions are under evaluation from 1 year of data (Birgand et al., in prep.). There are specific challenges inherent to water level measurements in field settings which have consequences on the uncertainties: lighting changes, camera movement, condensation on the lens, etc. (e.g. Bradley et al., 2002; Creutin et al., 2003; Hauet et al., 2008a,b; Muste et al., 2008). To interpret the field performance, however, the sources of uncertainty inherent with this novel technique must be described. Several studies propose image-based water level measurement techniques (Chakravarthy et al., 2002; Iwahashi et al., 2007; Shin et al., 2008; Yu and Hahn, 2010) but none describe in detail the sources of uncertainty associated with

* Corresponding author. Tel.: +1 919 208 1639; fax: +1 919 515 7760.
E-mail address: tegilmor@ncsu.edu (T.E. Gilmore).

0022-1694/$ - see front matter © 2013 Elsevier B.V. All rights reserved.
http://dx.doi.org/10.1016/j.jhydrol.2013.05.011

using images as raw data. This article aims at filling this gap. It describes the sources of uncertainties of this technique using data obtained in controlled laboratory conditions. Laboratory performance of this image-based technique is also compared to two commercially available water level measurement systems for reference.

2. Methods

2.1. Hardware

The camera used in the laboratory study is a rugged wireless surveillance camera (Microseven® Systems M7-RC550WS) equipped with IR lighting for night vision commercially available for less than $300.00 (in 2011). The target background required for the system can be built for less than $100. Access to an FTP server was used to gather data.

2.2. Technique principles

The water level measurement software developed at GaugeCam and available as freeware (http://www.gaugecam.com/product/downloads/) uses machine vision algorithms to measure water levels in two steps. First, water level is detected in the region of interest of an image where water draws a dark line against a white flat background. Second, the equation of the line in pixel coordinates is calibrated to real world coordinates thanks to benchmarks or fiducials, which are printed on the background and thus embedded in each image.

2.3. GRIME software details

GaugeCam Remote Image Manager Educational (GRIME) software was developed by GaugeCam to specifically address the challenges associated with measuring water levels in images. Water level detection is performed with a machine vision tool called an edge detector (ex. Marr and Hildreth, 1980; Torre and Poggio, 1986). On a defined area of an image where the water level draws a line against a flat background, each pixel column is scanned from top to bottom to detect sharp changes in the pixels gray scale using a non-parametric kernel tool. The sharpest gradients are saved as possible indicators of the water surface. The points for all the strong gradients in each column of an image are then evaluated to determine which set of those gradients best fit the expected angle of the water line (based on the rotation of the camera). Considerable amount of work is performed to ignore anomalous points, false lines, glint, etc. The best linear fit for the detected points is considered to be the water line, as shown in Fig. 1. Interestingly, this line's equation is expressed in pixel coordinates and may fall 'between' two pixels, resulting in sub-pixel resolution of the measurements.

To measure water levels in real world coordinates, a transfer matrix is calculated to relate the pixel to the world coordinates. Skew, perspective, and lens distortion come into play and are taken into account. Fiducials, or recognizable features (e.g. Fiala, 2010; Russ, 2011), are embedded at known real-world locations in the image, thus providing a reference between pixel and real world positions in each image. 'Bowtie' fiducials placed in two columns and four rows (Fig. 1) are automatically recognized by GRIME using blob analysis. A piecewise linear regression is then used to create the transfer matrix.

2.4. Sources of uncertainty

Detection and calculation of water level both involve uncertainty. Seven potential sources of uncertainty were identified in the lab: uncertainties associated with the image quality (image focus, image resolution, perspective, and lens distortion), uncertainties associated with the local environment (lighting effects, water meniscus) and uncertainties associated with the interpretation of the image by the software.

Obviously, one would want to obtain the clearest pictures possible as raw data. Most digital cameras available in the early 2010s can take at least several megapixel resolution pictures for images several MB in size. While this opens the possibility to have very sharp images, the memory size of such images is currently totally prohibitive, in terms of data volume and transfer time, for a system e.g. that would be placed in the field and remotely send images via cellular networks every 15 min. The camera for this study was purposely chosen so that images would not exceed 100 kb in size, hence limiting the resolution to around 250 kilopixels (details below).

Such images are not, as a result, as 'sharp' to the eye. Therefore, manually achieving optimal focus is not an obvious or a trivial task and is somewhat subjective. Additionally, focus differs within the same picture because the distance between the camera and e.g. the top and the bottom sides of the background differs, for a camera looking from the top. Focus is thus intrinsically linked to resolution and to perspective.

Representing a three dimensional environment onto a plane involves perspective. The software does account for that (e.g. Fig. 1B). The optics of the lenses themselves, however, add distortion. This is evident when straight lines (especially near the edges of an image) are displayed with a definite curvature on a picture. This effect is a more difficult to model and is only partially taken into account by GRIME. Higher focal length lenses provide less distortion and are thus preferable.

Because of surface tension forces, water forms a meniscus at the contact with a background. The size of the meniscus depends on the water and surface properties of the background. While e.g. a Teflon coated background would provide a different meniscus than PVC, it is the combined impact of the lighting and the meniscus size that creates the sharp change in pixel gray scale in an image. The lighting may change as a result of the angle and intensity of the incoming light source (e.g. sun, clouds, and IR illuminator at night).

The sources of uncertainties for image-based water measurement levels are thus intrinsically linked together. An accepted method to calculate uncertainties involves the classical propagation of error approach. A formal mathematical analysis of uncertainty can be performed for image analysis techniques (e.g. Kim et al., 2007), but only at considerable expense. Eq. (1) is the general equation for uncertainty with covariance (Kirkup and Frenkel, 2006).

$$u^2(y) = \sum_{i=1}^{n}\left(\frac{\partial y}{\partial x_i}\right)^2 u^2(x_i) + 2r(x_1,x_2)\frac{\partial y}{\partial x_1}\frac{\partial y}{\partial x_2}u(x_1)u(x_2) + 2r(x_1,x_3)\frac{\partial y}{\partial x_1}\frac{\partial y}{\partial x_3}u(x_1)u(x_3) + \cdots + 2r(x_i,x_j)\frac{\partial y}{\partial x_i} \times \frac{\partial y}{\partial x_j}u(x_i)u(x_j) + \cdots \quad (1)$$

where y is the measurand, $u(y)$ is uncertainty for the measurand, $u(x_i)$ is uncertainty of the input for x_i, $r(x_i,y_j)$ is the correlation coefficient between inputs for x_i and x_j, While rigorous, this approach also requires simplifying assumptions and estimates of individual uncertainties, which in our case are very difficult to separate.

A complete statistical analysis of all potential sources of uncertainty could theoretically be performed, but would require an impractical (and also costly) effort to fully isolate individual uncertainty components, and is beyond the scope of this article. Therefore, we have chosen to design efficient experiments that

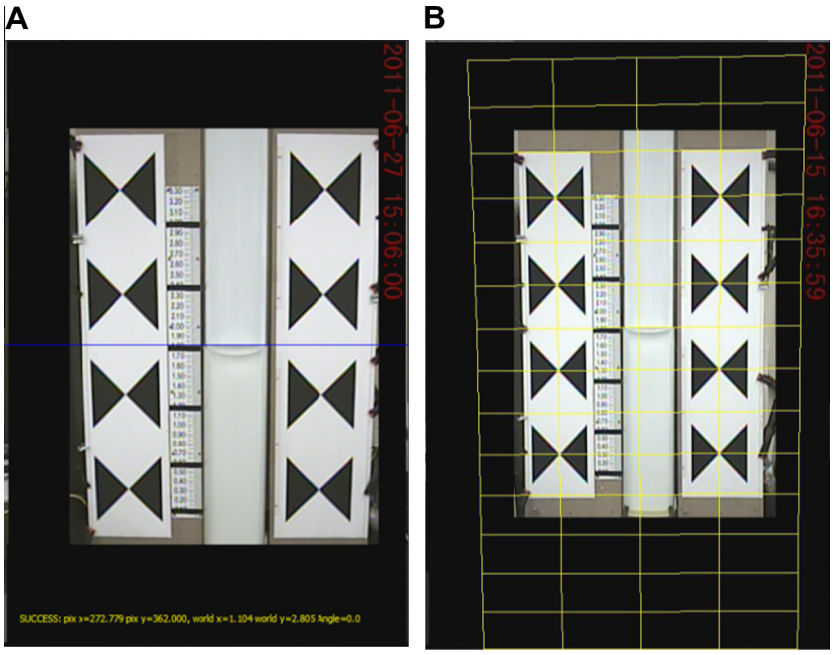

Fig. 1. Pictures of the experimental set up in the lab showing four vertical 'columns'. The outer columns contain the 'bowties' or fiducials; the left middle column is a gauge staff for visual measurement; the right middle column shows water lines in a clear acrylic cylinder (straight against flat background and curve against the cylinder's edge). The blue horizontal line in (A) represents the horizontal water line detected by the software. The yellow grid in (B), automatically centered on fiducials, is used to calculate the transfer matrix between pixel and real world coordinates (notice the perspective effect). (For interpretation of the references to color in this figure legend, the reader is referred to the web version of this article.)

incrementally introduce sources of uncertainty, from which we can infer the relative impact of the various sources. These experiments culminate in a final experiment in which all sources of uncertainty are introduced, thus giving an overall indication of uncertainty of the GaugeCam system in the laboratory setting.

2.5. Benchmark I

The Benchmark I experiment was designed to investigate image resolution as the source of measurement uncertainty. Eight sets of five screen capture images of a bowtie fiducial grid pattern with artificial water lines were created from a large format PDF file, as shown in Fig. 2. As such, the images had no distortion or perspective, and uncertainties found would reveal limitations in the software and in the image resolution effects such as pixelization, shown in Fig. 3. Each image set had a different resolution, with the smallest being 167 by 222 pixels and the largest being 932 by 1317 pixels.

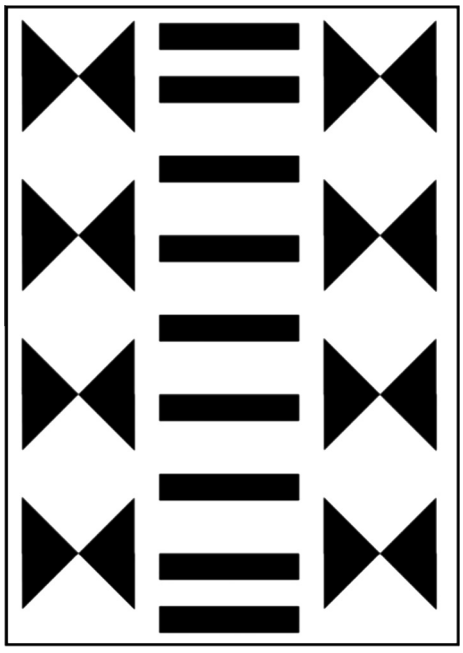

Fig. 2. Fiducial grid pattern (bowtie shapes) with artificial water levels (horizontal lines) used to assess uncertainties due to image resolution.

Artificial water level measurement results from GRIME were compared to the reference position of the artificial water lines. An error distribution was calculated by subtracting reference values from measured values. The standard deviation, mean bias and root mean squared error (RMSE) of the error distribution were also calculated. Based on the calculated GRIME output for each calibration, a value of cm per pixel was assigned to each set of images to indicate the number of centimeters in real-world height represented by each pixel in the image. The RMSE, standard deviation and mean bias were plotted against the cm per pixel values.

2.6. Benchmark II

In the second experiment referred to as Benchmark II, additional uncertainty sources including lighting effects, perspective and lens distortion were tested using actual images captured in the laboratory. The bowtie fiducials and artificial water level line pattern used in Benchmark I was printed on large-format white paper using a HP Designjet z5200 Postscript printer and affixed to a vertical background.

The wireless network camera (Microseven® Systems M7-RC550WS) captured images with maximum resolution of 720×480 pixels (NTSC) using a 1/3″ Sony Super HAD CCD sensor and 12 mm or 16 mm 1.3 megapixel lens. To minimize the picture sizes, only the region of interest centered around the fiducials was kept (e.g. Fig. 1). The image sensor was rotated 90° in the camera to maximize the use of the 720 pixel dimension in some cases. The camera was operated using M7CMS software, which provided

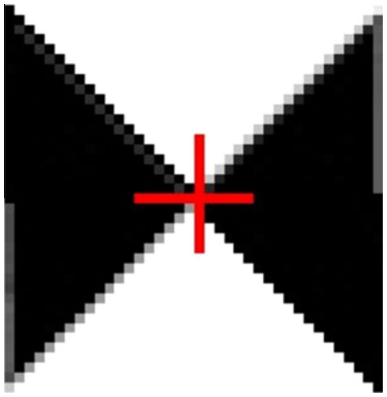

Fig. 3. Low resolution fiducial displaying pixelization. The center of the cross represents the pixel calculated to be the center of the fiducial associated with the known real world coordinates.

setup options to send images via FTP to an image management server with a Linux, Apache, MySQL and PHP (LAMP) stack. Images were then transferred to a laptop for processing in GRIME.

A mobile camera mount for the network camera was attached to a Unistrut® track located 2 m above center of the lowest fiducial set using Unistrut® trolleys, as seen in Fig. 4. Daytime and nighttime image sets ($n = 30$) were captured at various horizontal distances from the background target, ranging from 2.5 m to 14.85 m, perpendicular to the target surface. The camera was also mounted on a separate track that was parallel to the target surface and 2.5 m horizontal distance from the target. From this rail, camera posture (or, offset) angles of 10°, 20° and 30° were investigated.

Daytime lighting consisted of ambient light from a laboratory window as well as fluorescent tube lighting in the laboratory. Nighttime illumination was from the infrared light-emitting diodes (IR-LEDs) onboard the Microseven® camera, with fluorescent lighting turned off and all laboratory windows covered with black material. The only light sources in the lab for night images were the IR lighting and ambient light from computer monitors located approximately three meters from and oriented away from the water level bench.

Images were processed in GRIME as described for Benchmark I. A cm per pixel value was recorded for each image set, since each camera position produced a different resolution image. Statistical analysis was performed for each cm per pixel values as described in Benchmark I.

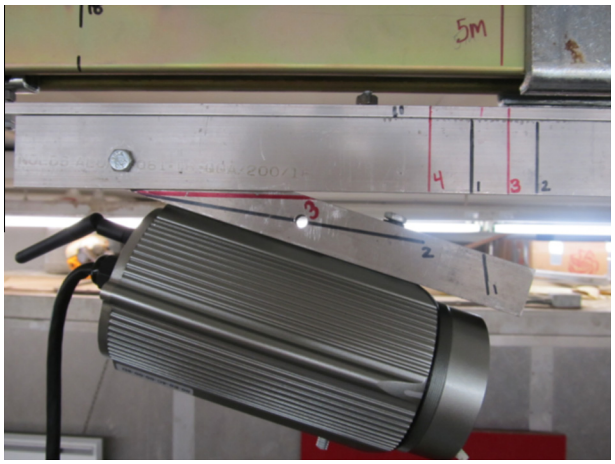

Fig. 4. Side view of the network camera and mount where angles and distance to the target were adjusted.

2.7. Water level

The final water level experiment included all previous sources of uncertainty and added the effect of the water meniscus. A clear water level cylinder equipped with a pumping and draining system was inserted into a cutout of the background used for Benchmark II images (Fig. 1). The water level cylinder was a clear acrylic cylinder with an outside diameter of 20.3 cm and wall thickness of 0.6 cm. A white flat background (Coroplast®) was inserted inside the acrylic cylinder and placed in the same plane as the cutout background. Water was pumped into the water level cylinder using a submersible pump and was drained through a drain hose connected to the bottom of the water level cylinder. The drain hose was mounted in an inverted U-shape so the water would siphon out of the cylinder only after the water level exceeded the maximum height of the drain hose. The tube refilled and drained repeatedly as long as the pump was operating. A valve installed in the outlet hose allowed for controlled descent of the water level. This allowed the upward meniscus to be maintained while setting various water levels. Fiducials were precisely placed at known locations and flat against the cutout background to be in the same plane as the inserted white Coroplast® background. A Style A staff gauge with length of 1.01 m was permanently and vertically mounted next to the water level tube and used to make visual readings.

Images were captured with the camera located at a horizontal distance of 4, 5, 6 and 7 m from the background target. These horizontal distances translate to 16°, 12°, 10° and 9° line of sight angle between the horizontal camera rail and the center of the top fiducial, respectively. To the center of the bottom fiducials, line of sight angles were 30°, 23°, 19° and 16°, respectively. Fig. 5 depicts line of sight angles for the 6 m camera position.

The front surface of the camera lens was set to the nominal horizontal distance from the background target for each horizontal distance. The camera mount was clamped to the Unistrut® track to prevent movement. The camera was focused by observing the image in the M7 CMS viewer and manually adjusting the lens on the camera until optimal focus was achieved.

Water level images were collected by first visually setting and manually recording the reference water level. The bottom of the water meniscus was aligned with the top of the chosen mark on the staff gauge located next to the water level cylinder. This could be adjusted quite precisely thanks to the magnifying effect of water in a cylindrical container and we estimate that the uncertainty on the position of the water level was within half a millimeter of the reading. Eleven images were captured at 2-s intervals. The water level was then lowered to the next position, and the process was repeated. After reaching the lowest water level, the water was pumped slightly above the intended position, then lowered to the desired water level to preserve the upward water meniscus. A macro-level reference image was recorded for each water level

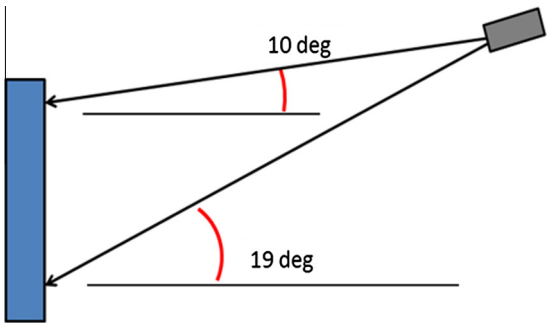

Fig. 5. Line of sight angles for the top and bottom fiducials for the camera positioned 6 m away from the target.

using a standard digital camera. The initial set of water level images were recorded with daytime lighting at 6 m horizontal distance from the target. Fifteen repetitions of seven water levels were completed from this distance. Given the very low variability in measurements observed in the fifteen repetitions, the number of repetitions was lowered to five repetitions for the other camera positions for which data is presented in this article.

Edge line (water level) detection settings were determined for each camera position by trial and error to produce the best results for both day and night images. 'Threshold' (Table 1) sets the minimum rate of change in grayscale value required for an edge point to be valid. 'Minimum percentage points' sets a minimum percentage of columns in which a valid edge point must be found in order to consider the resulting linear regression as valid. 'Kernel size' is the number of pixels in the non-parametric custom kernel. 'Which edge' defines whether the first line found is considered the measurement, or if the line with maximum gradient is considered the measurement. 'Polarity' indicates whether edges transitioning from high to low or low to high grayscale values are found. 'Edge Line Outlier Removal' removes stray edge points from the image by first calculating a regression line for all found edge points, then eliminating any points that are a user-specified distance from the regression line. GRIME also allows for outlier control to be applied iteratively, removing outlying edge points then applying linear regression to the remaining point constellation before checking for additional outliers. 'Angle control' compares the regression line angle from a user-specified nominal angle and either accepts or rejects the measurement based on a user-specified value. A single settings file was utilized for all images collected at each camera position. Outlier detection and line angle control were used for the 7 m images, as the nighttime lighting images contained a disruptive glare and reflection from the IR lighting. Settings for the 7 m images are provided in Table 1.

Camera positions of 4, 5 and 6 m resulted in similar, but less disruptive, glare and reflection for nighttime lighting images. Therefore, outlier detection and line angle control were not necessary for processing the images taken between 4 and 6 m. Images were also checked for camera movement using the camera motion detection feature in GRIME. If significant camera movement was detected using this feature, a new calibration was performed for each set of images for which the camera was stationary. Once calibration and edge line settings were established and saved, images were processed. For water level measurements the mean value from the 11 images was taken as the measured value. The angle control feature of GRIME rejected some of the 7 m measurements. In this case, the measured value was based on one or more water level measurements not rejected by GRIME.

2.8. Instrument comparison

A comparison of the image-based water level measurement system with two commercially available water level measurement devices (pressure transducers) was conducted for the final experiment. Seventy measurements were recorded concurrently by the transducers and the image-based system using daytime lighting. Transducer 1 was an INFINITIES USA, INC calibrated for a 7.62 m (25 ft) range, with elevation input adjusted so that the transducer measurement matched a visual measurement of 0.85 m on the staff gauge. Transducer 2 was an Onset HOBO Model U20-001-04 calibrated for a 3.96 m (13 ft) range. Transducer 2 measurements were postprocessed to match a visual measurement of 0.85 m. Transducer and Microseven® camera clocks were synchronized in order to minimize discrepancies between measurements. Water level was set manually, as in the other water level tests, while transducers recorded measurements every 30 s. Each water level position was held constant for 2–3 min resulting in 4–6 measurements taken by the transducers while the water level was stationary. Other measurements were removed from the data set before comparing with image-based water level measurement system results.

Table 1
GRIME settings for 7 m images.

Parameter	Setting
Threshold	15
Min% points	20
Kernel size	7
Which edge	First
Edge polarity	Falling
Edge line outlier removal	0.50 pt, 4 passes
Angle control	0.00, ±5.00°

3. Results and discussion

3.1. Benchmark I – effects of resolution

All images for this experiment were obtained from screen captures of a pdf file that contained the fiducials and the artificial water lines. For a particular resolution, five images were captured and each artificial water line was thus detected five times. First it should be noted that for a particular image, the software would always give the same results. The uncertainty for a particular measurement and image came from actual differences in the pixelization of the fiducials and the artificial water levels (e.g. Fig. 3). It was hypothesized that the random screen captures would generate differences among images. The differences in cm between the measurements and the reference values for several resolutions are illustrated in Fig. 6. For each artificial water level (nine x coordinates), five measurements are plotted although in many instances, only one or two symbols is/are visible, the others being superimposed. Fig. 6 shows that artificial water levels can be randomly over or underestimated, although for the 0.23 and 0.26 cm/pixel, the levels were always overestimated. This is most likely due to the way the pixelization is performed on the screen and/or during screen capture. Fig. 7 shows that the variability and the size of the errors seems to decrease as the cm per pixel value decreased. In other words, the variability of the errors decreased as resolution of the image increased, which was expected.

Errors shown in each plot in Fig. 6 (in addition to other resolution results) were compiled into three indicators, the root mean square error (RMSE), the mean bias and the standard deviation. RMSE was calculated by taking the square root of the random error (standard deviation of the bias) and the systematic error (mean of the bias) combined in quadrature (described by Taylor, 1997). These indicators were plotted against the image resolution, in terms of real-world cm per image pixel, in Fig. 7. We consider the RMSE values for Benchmark I as the theoretical minimum error, because the only source of uncertainty was image resolution. Results show that the RMSE did generally increase as a function of decreasing resolution and did not exceed 2 mm, although the relationship was somewhat erratic. This was probably due to the way pixelization was done during image captures on the computers used.

3.2. Benchmark II – effects of position, distortion, and lighting

Benchmark II error distributions presented in Fig. 8 display greater variability than Benchmark I. Results are separated into day and night lighting scenarios in order to demonstrate that results were similar for each case. Bias was greatest in magnitude

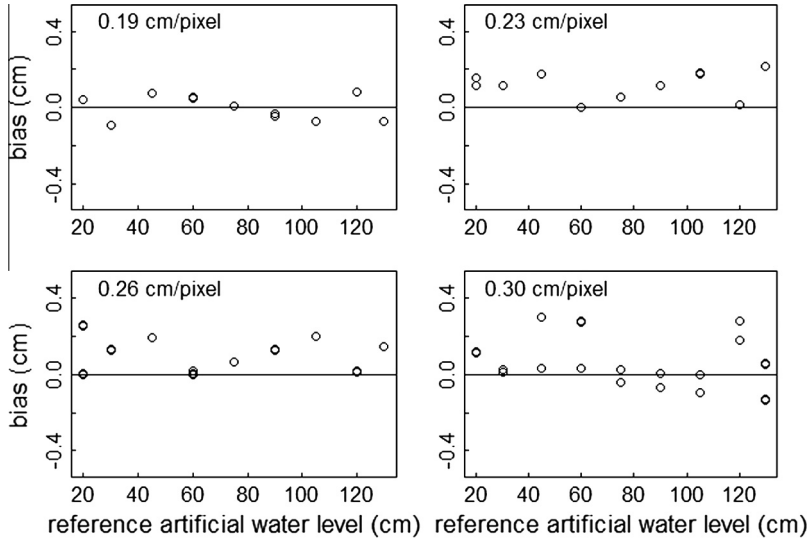

Fig. 6. Selected error distributions for Benchmark I.

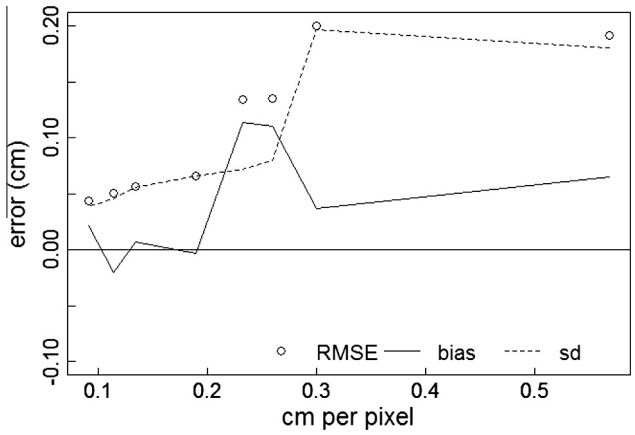

Fig. 7. Uncertainty (bias, precision – SD and RMSE) on artificial water levels due to the image resolution alone (Benchmark I experiment).

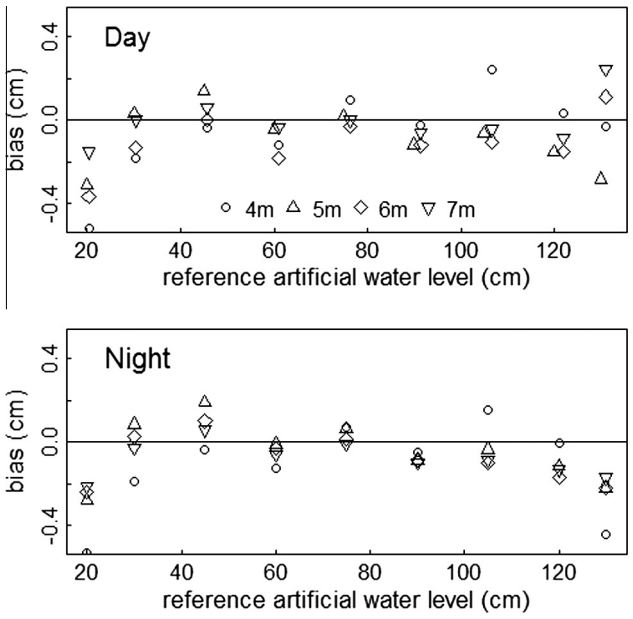

Fig. 8. Measurement errors for day and night lighting obtained on artificial water levels as a function of camera distance to the target and reference water level.

at the 20 cm and 130 cm artificial water levels. Those levels extended below and above the fiducial grid pattern and were obtained by extrapolation in the GRIME calibration calculation. In the version of GRIME used, the extrapolation method did not fully account for perspective and increased lens distortion as the artificial water level approaches the edges of the image. The results from artificial water levels located within the fiducial grid pattern (30–120 cm), however, indicate that perspective and lens distortion were well modeled by the GRIME calibration.

Camera positions from 4 m to 7 m produced ideal results compared to other camera positions for Benchmark II. Camera positions closer than 4 m (data not shown) caused the fiducials to appear very close to the edge of the image and therefore induced greater error due to lens distortion, particularly at the highest and lowest artificial water levels previously mentioned. Images taken at offset (10°, 20° and 30°; data not shown) posture angles not only caused the fiducials to appear near the edge of the image, but potentially induced additional error due to the effects of perspective.

RMSE for Benchmark II, displayed in Fig. 9, are generally less than 2 mm for all resolutions and tended to be similar for day and night lighting scenarios. The image-based water level measurement system slightly underestimated the artificial water level for the camera positions tested. The RMSE at 0.26 cm per pixel stands out in Fig. 9. The images at this resolution were captured using a 12 mm lens at 4 m, as opposed to the 16 mm lens used for the three other camera positions. We believe that the increased lens distortion associated with the 12 mm lens contributed to the relatively high error for this resolution. Further support for this idea is seen in Fig. 8, as the most extreme errors, particularly at 20 cm and 130 cm, are for the 4 m camera position (with the exception of 130 cm in using day lighting). Considering the remaining three RMSE values, a surprising trend of decreased error with decreased image resolution emerges. This may be explained by the reduced impact of lens distortion as the fiducial grid pattern and artificial water lines shrank toward the center of the image.

Another unanticipated result is that the RMSE values at 0.33 cm per pixel (7 m camera position) were actually lower than the theoretical minimum error discussed in Benchmark I results. This is attributed to the difference in gray scale gradients in the screen captured and real images. In the screen captured images, pixelization resulted in relatively sharp changes between absolutely white

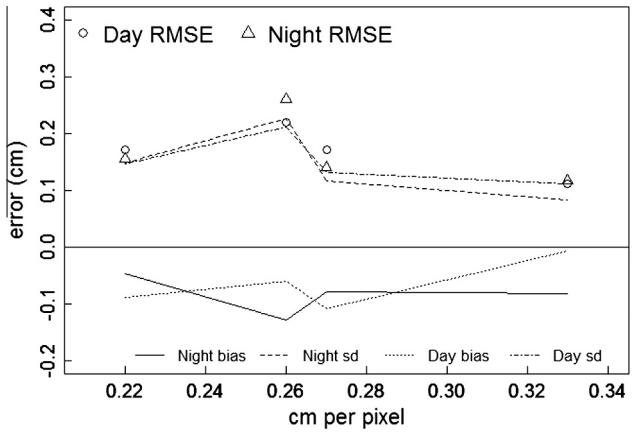

Fig. 9. Uncertainty (bias, precision and RMSE) on artificial water levels due to focus, image resolution, perspective, and image distortion (Benchmark II experiment).

pixels and the black ones. For the real images, the gradient between the white pixels (actually light gray) and the black pixels (dark gray) were not as abrupt, for which the software was well suited. As a result, both the detection of the fiducial centers and the line edges were apparently detected with greater accuracy than for the Benchmark I pictures.

3.3. Water level experiment – additional effect of water meniscus

Error distributions from the water level experiment are presented in Fig. 10 for seven water levels all included within the fiducial range. With the exception of the 4 m results, the tendency to overestimate (positive bias) the control water level height decreases as water level height became greater. The greater image distortion associated with the 12 mm lens might explain the opposite trend for the 4 m results. In all cases, a change in bias is evident as water level changes. This is a trend not evident in the Benchmark I or II experiments. As a result, we feel this trend may be explained by a change in the measurement system perception of the water meniscus as the line of sight angle changed, as described in Fig. 5.

The bias values in Fig. 10 indicate an increasing tendency to overestimate water level as distance between the camera and the target increases, presumably due to the height of the water meniscus (2–3 mm). The divergence of day and night values is especially noticeable at values of 0.26 cm/pixel (6 m) and greater (Fig. 11) and for all water heights (Fig. 10). We attribute this divergence is attributed to the meniscus and to glare and reflection from the IR lighting source during nighttime image capture. The glare might have been removed by adjusting the position of the light source. However, our objective was to test the system with a commercially available camera which had onboard IR lighting, so we did not make changes to the lighting configuration.

Interestingly, the images taken with the 16 mm lens induce a systematic bias increasing with the angle (the lower the water level, the greater the angle) between the camera and the water line. This systematic bias is not prevalent for images taken with the 12 mm lens (Fig. 10). The results with the 16 mm lens make sense as a dark line should appear on the image, because of the upward meniscus, a little higher than actual stage (positive bias of 1.5–2 mm) and should change somewhat with the camera–water line angle and the lighting. The lack of bias is suspicious using the 12 mm lens and might be just coincidental where the image distortion error was somehow compensated. This further confirms that least image distortion is preferred.

Based on these results, the meniscus seems to induce a systematic bias of 1.5–2 mm. This variation can be minimized by minimizing the angle between the camera and the perpendicular to the background plane (e.g. less than 14° corresponding to higher water levels in Fig. 10). This bias should be subtracted from the readings of this image-based technique to lower the overall error and to lower the probability of systematic overestimation. When visually measuring water levels on images from the field, one would have to experimentally estimate the bias and subtract it to the visual and automatic readings.

Although these results were obtained in a clear acrylic cylinder in the lab and cannot be directly translated to performance in the field, it seems that this technique, provided that correction for meniscus bias be applied, has the potential to reach uncertainties of ±3 mm. This must be confirmed with field measurements (Birgand et al., in prep.).

3.4. Instrument comparison

Image-based measurements of water level compared favorably with two commercially available transducers, as seen in Fig. 12. One transducer tended to overestimate while the other underestimated, which highlights the difficulty of accurately setting offset

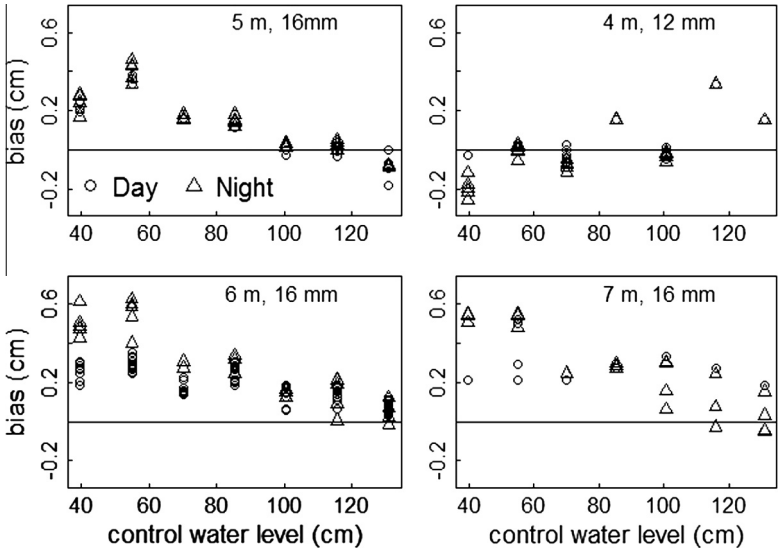

Fig. 10. Error distribution for day and night conditions on seven actual water levels in clear cylinder.

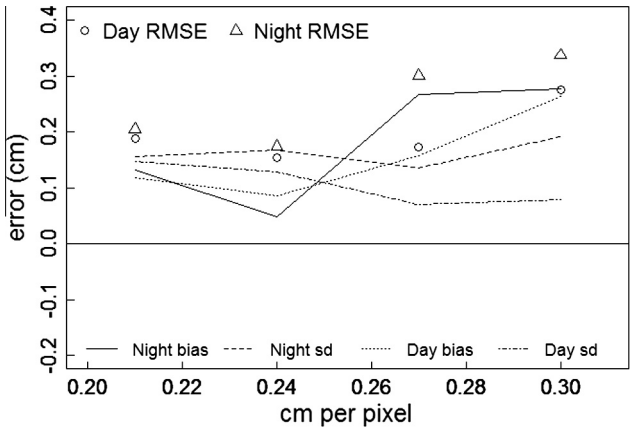

Fig. 11. Uncertainty (bias, precision and RMSE) on actual water levels due to all sources of uncertainties (Water level experiment).

values for water level instruments. The uncertainty ranges (represented by the extent of the whisker plot in Fig. 12) are higher for the pressure transducers. This could be attributed to the response time lags of this technology. Although the results were obtained for day lighting in Fig. 12, the comparison should hold at night given the similar RMSE values for day and night lighting in Fig. 11.

3.5. Lessons learned from measurement uncertainties observed in the lab

Image-based water level measurements have the potential to be wide spread in the near future because the image acquisition, transfer and storage technologies already exist, and cost (already reasonable), will keep decreasing. Images also provide an unmatched way to visually verify suspicious measurements, but for a viable system the vast majority of measurements should not require visual verification. It is thus essential to know the expected uncertainties inherent to this technique and the care needed to obtain best results.

Results show that image resolution and the water meniscus are the major sources of uncertainty, provided that care has been taken to minimize the effects of image distortion. Results show that higher image resolution gives, as expected, better results, although a rather narrow range of resolutions were tested with water (0.2–0.35 cm/pixel), corresponding in the worst case to a camera fitted with a 16 mm lens placed 7 m away from the target. Poorer resolution as tested in the benchmark I experiment (0.5 cm/pixel) should lead to larger uncertainties. The impact of poorer resolution on water level measurements in the lab could not be assessed as the diameter of the cylinder tested did not provide a wide enough water line for the software to recognize when the camera was placed further away. Image lighting and its impact on water meniscus weighed comparably on the uncertainty for the distances tested showing that the measurement bias can change significantly if the angle of view changes a lot (e.g. 10–19° in Fig. 5) across the measurement spectrum. The way to minimize such angles are thus to place the camera at a minimum angle to the perpendicular of the background plane. Practically, this may involve placing the camera as low as possible to the maximum water level expected and to place the camera further away. This recommendation also goes towards improved focus.

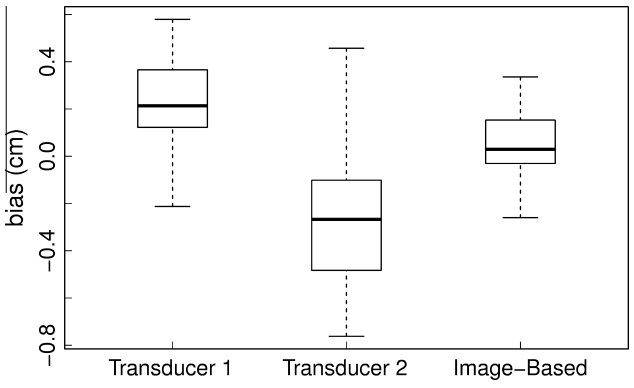

Fig. 12. Comparison of water level measurement uncertainty ranges between the image-based system and two pressure transducer based systems in the lab during daytime.

Image distortion was shown to potentially add to uncertainty. In the original experimental design, offset angles (10–30°) to the target were tested for distances of 3 m or less to the target. Because of the proximity, the images were highly distorted and the results judged unreliable. Similarly, the poorer results obtained using the 12 mm lens at a distance of 4 m to the target were attributed to lens distortion. Best results in the Benchmark II experiment were obtained at 7 m (Fig. 8), suggesting that less image distortion might be just as or even more important than image resolution in the acceptable resolution range (0.2–0.35 cm/pixel). It is thus theoretically preferable to obtain rather 'flat' pictures using a deeper focal length camera placed further away from the target. The results also show that, when distortion was minimized, the software satisfactorily corrected for perspective.

The image-based system compared favorably to the pressure transducers tested in the lab. This confirms that this technique has the potential to be used and perform at comparable levels, although this needs to be confirmed in the field. In all cases, it does provide the unmatched ability to visually read and interpret the raw data.

4. Conclusions

Our approach in this lab study was to identify and evaluate the impact of potential sources of uncertainty that affect image-based water level measurements. These factors include image focus and resolution, lighting effects, lens distortion, perspective and the water meniscus. Image resolution and water meniscus, for the distances tested, were the two most important and consistent sources of uncertainty. The first experiment results (Benchmark I) indicate that for a wide range of image resolutions, uncertainty (±RMSE) less than ±2 mm is consistently achieved. Despite the addition of lighting effects, lens distortion and perspective in the second experiment (Benchmark II), RMSE remained below 2 mm with the exception of 4 m images captured with a 12 mm lens, suggesting that the software satisfactorily took into account perspective issues, provided that image distortion was minimal. In the third experiment, Water Level results for day lighting, which included no extrapolated water level measurements above or below the fiducial pattern, also met the 2 mm criteria. Night Water Level RMSE exceeded 3 mm at the 6 m and 7 m camera position, but the strong mean bias component (>2 mm) at these camera positions was attributed to glare from the IR lighting, which is a correctable issue. Error ranges for two commercially available water level measurement transducers (calibrated for a range substantially greater than target background height) exceeded the image-based water level measurement error range. Based on these results, we conclude that with reasonable care to reduce the known sources of uncertainty, and by subtracting bias induced by the meniscus, it may be possible to measure water level within ±3 mm using the system described in this article and in the lab.

The obvious next step is to quantify uncertainties in a field application of the image-based water level measurement system. The additional challenges (based on ongoing, unpublished field feasibility studies) which include camera movement or shifting background, ambient lighting or shadow effects, floating debris, biofilm or sediment buildup on the target background and dirty lenses, are the subject of another article (Birgand et al., in prep.).

Acknowledgements

The authors gratefully recognize Kelly Chapman for lab assistance and Christian Chapman for server configuration. Thanks also to Ihab Ghali for capturing benchmark images.

References

Birgand, F., Gilmore, T.E., Chapman, K.W., Brown, A., in preparation. Evaluation of the GaugeCam image-based water level measurement system in the field.

Bradley, Allen A., Kruger, Anton, Meselhe, Ehab A., Muste, Marian V.I., 2002. Flow measurement in streams using video imagery. Water Resour. Res. 38 (12), 1315.

Chakravarthy, S., Sharma, R., Kasturi, R., 2002. Noncontact level sensing technique using computer vision. IEEE Trans. Instrum. Meas. 51 (2), 353.

Creutin, J.D., Muste, M., Bradley, A.A., Kim, S.C., Kruger, A., 2003. River gauging using PIV techniques: a proof of concept experiment on the Iowa river. J. Hydrol. 277 (3–4), 182–194.

Fiala, M., 2010. Designing highly reliable fiducial markers. IEEE Trans. Pattern Anal. Mach. Intell. 32 (7), 1317–1324.

Heiner, B., Barfuss, S.L., Johnson, M.C., 2011. Conditional assessment of flow measurement accuracy. J. Irrig. Drain. Eng. – ASCE 137 (6), 367–374.

Hauet, Alexandre, Creutin, Jean-Dominique, Belleudy, Philippe, 2008a. Sensitivity study of large-scale particle image velocimetry measurement of river discharge using numerical simulation. J. Hydrol. 349 (1–2), 178–190.

Hauet, Alexandre, Kruger, Anton, Krajewski, Witold F., Bradley, Allen, Muste, Marian, Creutin, Jean-Dominique, Wilson, Mark, 2008b. Experimental system for real-time discharge estimation using an image-based method. J. Hydrol. Eng. 13 (2), 105–110.

Iwahashi, M., Udomsiri, S., Imai, Y., Muramatsu, S., 2007. Water level detection for functionally layered video coding. In: 2007 IEEE International Conference on Image Processing, vols. 1-7885-888.

Kim, Y., Muste, M., Hauet, A., Bradley, A., Weber, L., Koh, D., 2007. Uncertainty Analysis for LSPIV In-situ Velocity Measurements, Presented at 32nd Congress. Int. Assoc. Hydraul. Eng. Res., Venice, Italy.

Kirkup, L., Frenkel, R.B., 2006. An Introduction to Uncertainty in Measurement Using the GUM (Guide to the Expression of Uncertainty in Measurement). Cambridge University Press, New York.

Marr, D., Hildreth, E., 1980. Theory of edge-detection. Proc. Roy. Soc. Lond. Ser. B – Biol. Sci. 207 (1167), 187–217.

Muste, M., Fujita, I., Hauet, A., 2008. Large-scale particle image velocimetry for measurements in riverine environments. Water Resour. Res. 44 (4), W00D19.

Rantz, S.E. et al., 1983. Measurement and Computation of Streamflow. Measurement of Stage and Discharge, vol. 2. U.S. Geological Survey Water-Supply Paper 2175. U.S. Dept. of Interior, Washington, DC, GPO.

Russ, J.C., 2011. The Image Processing Handbook, sixth ed. CRC Press, Boca Raton, Fl.

Shin, I., Kim, J., Lee, S., 2008. Development of an Internet-based Water-level Monitoring and Measuring System using CCD Camera. Icmit 2007: Mechatronics, Mems, and Smart Materials, Pts 1 and 2 6794Q7944-Q7944 (Art. No. 67944Q).

Taylor, J.R., 1997. An Introduction to Error Analysis: The Study of Uncertainties in Physical Measurements. University Science Books, Sausalito, CA.

Torre, V., Poggio, T., 1986. On edge-detection. IEEE Trans. Pattern Anal. Mach. Intell. 8 (2), 147–163.

Yu, J., Hahn, H., 2010. Remote detection and monitoring of a water level using narrow band channel. J. Inform. Sci. Eng. 26, 71–82.